Title

Reduced Electromagnetic Edge Scattering Using Inhomogeneous Anisotropic Impedance Surfaces

Journal

IEEE Transactions on Antennas and Propagation, 65(3)

ISSN

0018-926X

Authors

Hou, Haijian
Long, Jiang
Wang, Junhong
et al.

Publication Date

2017-03-01

DOI

10.1109/tap.2016.2647681

Peer reviewed

Reduced Electromagnetic Edge Scattering Using Inhomogeneous Anisotropic Impedance Surfaces

Haijian Hou, Jiang Long, *Student Member, IEEE*, Junhong Wang, *Senior Member, IEEE*, and Daniel F. Sievenpiper, *Fellow, IEEE*

***Abstract*— Electromagnetic scattering characteristics highly depend on the geometry and material property of the scatterers. In particular, electromagnetic wave scattering occurs at the discontinuity of the propagation path, such as the edge of a scatterer. In this paper, the edge scattering from a triangular object is largely reduced by patterning the triangular surface with inhomogeneous and anisotropic impedance surface. Because surface waves propagate toward the direction with the lower surface refractive index on an anisotropic surface, the direction of the wave propagation can be controlled by designing the distribution of the refractive index. Consequently, the proposed anisotropic impedance surfaces can make the current flows toward or away from the edge so that the edge scattering can be reduced or redirected to a different angle. For demonstration, anisotropic unit cells are analyzed and designed. Also, the anisotropic impedance surfaces are simulated, fabricated, and measured. Here we propose two types of impedance profiles, which are capable of changing the surface current direction either toward or away from the scattering edge. The experimental measurement demonstrates a 7–10 dB edge scattering reduction.**

***Index Terms*— Anisotropic surface impedance, electromagnetic metamaterials, metasurface, radar cross sections (RCSs), scattering.**

I. Introduction

ARTIFICIAL impedance surfaces (AISs) have a surface impedance which is controlled by the geometry and arrangement of subwavelength metallic patches on a grounded dielectric substrate. They are part of a class of structures generally called metasurfaces, which include electromagnetic bandgap (EBG), surfaces, high impedance surfaces, artificial materials, and so forth. Many applications have been explored, including antennas, lenses, and waveguides. When used in antenna applications, they can be used to improve gain, reduce side lobes, and improve isolation by reducing the surface wave coupling between the multiple antennas. For example, low radar cross section (RCS) has been demonstrated using microstrip antennas combined with an EBG structure [1]–[3]. In lens applications, AISs have been implemented to control the pattern of refractive index, which leads to the design of fish eye lenses and Luneburg lenses [4]–[7]. Also, a surface waveguide can be created by using a strip of high index AIS surrounded by low index surfaces [8]. Moreover, anisotropic impedance surfaces have been used to achieve lower RCS by using the concepts such as cloaking, transformation optics, control of scattering or guiding of wave propagation, and rotation of the electromagnetic field [9]–[14].

When a wave impinges upon a surface such as a metallic sheet, reflection from the surface and scattering from the edges are induced. For antenna engineers, it is crucial to reduce the energy scattered from the edges in order to control the radiation pattern [15]. In this paper, we are primarily focused on the scattering of the transverse magnetic (TM) surface waves. Other related researches have involved patterning a hard and soft surface onto a metal sheet to create an artificial boundary which is able to change the direction of backward scattering [16]. In this paper, a novel approach is proposed to reduce the scattering from edges by using anisotropic impedance surfaces [17]–[19] to redirect the surface wave propagate toward or away from the edges.

The scattering properties of an object are controlled by the combination of material property and geometry, such as by using absorbing materials, or configuring its shape so that waves are scattered to specific angles. For antennas, this can involve designing the size and shape of the ground plane to achieve specific radiation pattern goals, leading to designs that are not necessarily optimum from the perspective of other engineering tradeoffs, such as size, weight, or aerodynamics. The basic concept of this paper is that we can control the specular reflection from a particular edge by tailoring the surface impedance around that edge with inhomogeneous anisotropic impedance surfaces. Specifically, it is known that the reflected wave can be reduced by changing the angle of the incident wave. To change the incident angle, we can not only physically change the edge orientation, but also change the wave propagation direction relative to the edge geometry. The latter provides an additional tool for the electromagnetic designers beyond simply changing the geometry of the surface. In this paper, we demonstrate this concept with a simple triangular scatterer by reducing specular reflection from the hypotenuse.

When a plane wave impinges on a metal surface, current is excited on the surface, creating radiation from the edges [20], [21]. As shown in Fig. 1(a), when an incident

Manuscript received January 25, 2016; revised November 24, 2016; accepted December 9, 2016. Date of publication January 4, 2017; date of current version March 1, 2017. This work was supported in part by the Air Force Office of Scientific Research under Contract FA9550-16-1-0093 and in part by the National Natural Science Foundation of China (NSFC) Project under Grant 61271048 and Grant 61331002.

H. Hou is with Beijing Jiaotong University, Beijing 100011, China, and also with the Applied Electromagnetics Research Group, University of California at San Diego, La Jolla, CA 92093 USA (e-mail: 12111005@bjtu.edu.cn).

J. Long is with Skyworks Solution Inc., Woburn, MA 01801 USA (e-mail: jilong@ucsd.edu).

J. Wang is with Beijing Jiaotong University, Beijing 100011, China (e-mail: wangjunh@bjtu.edu.cn).

D. F. Sievenpiper is with the Applied Electromagnetics Research Group, University of California at San Diego, La Jolla, CA 92093 USA (e-mail: dsievenpiper@eng.ucsd.edu).

Color versions of one or more of the figures in this paper are available online at http://ieeexplore.ieee.org.

Digital Object Identifier 10.1109/TAP.2016.2647681

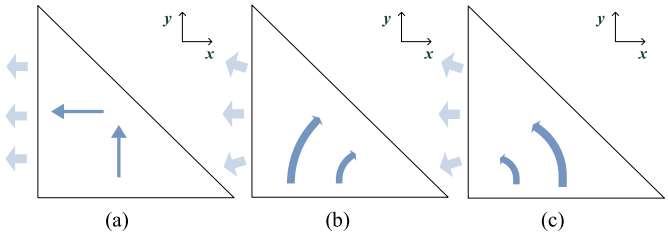

Fig. 1. Scattering manipulation. A plane wave enters the three different models including metal and anisotropic impedance surfaces. Different scattering behaviors are created by controlling the incidence angle on the hypotenuse edge of the triangle. (a) Bare metal. (b) Anisotropic AIS guiding surface waves toward the hypotenuse edge. (c) Anisotropic AIS guiding surface waves away from the edge.

plane wave propagating along the positive y-direction, strong scattering peak toward $-x$-direction is produced owing to the reflection at the hypotenuse of the triangle surface. Fig. 1 illustrates the concept of this paper: when the wave is steered toward the edge, we would expect the scattered energy to be stronger toward directions normal to that edge. When the wave is steered away from the edge, it hits the edge closer to a grazing angle, and it is thus expected that the scattered energy will be directed toward the grazing angles. Here, a simple triangle structure was chosen because it is straightforward to identify the scattering peak, which enables us to study patterning techniques to control the scattering behavior.

In order to reduce the scattering peak of a triangle structure, the geometric reflection from its hypotenuse needs to be altered. Because the reflection angle is determined by the phase progression of the surface waves along the edge, it can be controlled by changing the direction of the incident surface waves relative to the orientation of the hypotenuse without modifying the physical geometry of the hypotenuse. This can be realized by an anisotropic AIS, which is able to guide the surface waves toward or away from the hypotenuse, the edge causing the reflection. Surface waves on impedance surfaces can be controlled either by building discrete waveguides, or by using anisotropy. On an anisotropic surface, the waves will tend to follow the direction of lowest impedance, or refractive index, according to the principle of least time [22]. Specifically, the surface wave is guided toward the edge as illustrated in Fig. 1(b) when the low refractive index is rotated toward the edge. On the contrary, when the low refractive index is rotated away from the edge, surface waves avoid the edge as shown in Fig. 1(c). In either case, the waves hit the edge at a different angle either near normal or grazing and both can reduce the scattering toward the regular specular angle. In this paper, we study both cases, and demonstrate that both cases are effective at controlling scattering from the edge.

The remainder of this paper is organized as follows. Section II discusses the theory of anisotropic AISs and design of the unit cell. Characteristic parameters of the proposed anisotropic AIS are also discussed in Section II. Based on these characteristics, both discontinuous and continuous patterns are introduced in Section III. For the discontinuous case, the surface is divided into several sections. For the continuous case, the impedance is varied smoothly across the surface. Simulation and measurement results are presented

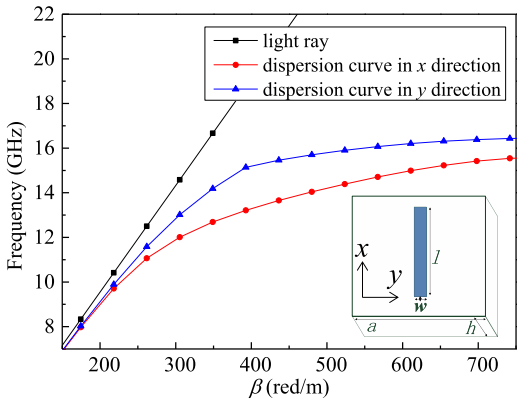

Fig. 2. Unit cell model and dispersion curves. Configuration parameters: the length of unit cell $a = 4$ mm, length of dipole short edge $w = 0.3$ mm, length of dipole long edge $l = 3$ mm, height of substrate $h = 1.27$ mm. The permittivity of the substrate is 10.2 and the permeability of the substrate is 1. The black line represents free-space propagation, and dispersion curves below this light line correspond to bound surface wave modes.

and discussed in Sections IV and V. In Section IV, the RCS of anisotropic AIS and a simple copper triangle are compared and analyzed. In Section V, surface wave results are calculated using near-field measurement results, and scattering characteristics are obtained by far-field measurement

II. Anisotropic Impedance Unit Cell

A. Anisotropic Surface Unit Cell

An anisotropic AIS is created by covering a grounded dielectric substrate with a pattern of metallic shapes [23]–[26]. In this paper, a dipole shaped rectangle is printed on Rogers 6010 substrate with a copper ground. This particular pattern is chosen because of its simplicity, its ease in creating a high degree of anisotropy, and the fact that it can be rotated in any direction within its square unit cell. In Fig. 2, the unit cell is shown in Cartesian coordinates, in which the short edge of the copper rectangle is in y-direction with length $l = 0.3$ mm and the long edge is in x-direction with $w = 3$ mm. The period of the unit cells is 4 mm, which is longer than the diagonal of the copper patch, so adjacent patches does not touch each other no matter how they are rotated.

The impedance of the anisotropic AIS is a function of the geometry of the unit cell, the substrate permittivity, as well as the incident wave direction. In this paper, a rectangle shaped unit cell is discussed and its behavior is similar to the dipole unit cell which can be used to make hard and soft surfaces [24] each a kind of highly anisotropic impedance surface. A TM polarized surface wave sees high impedance when propagating along the longitudinal edge of the rectangle patch, whereas low impedance is seen by TM waves when the wave is traveling in transverse direction [18], [24].

As discussed in Fig. 1, strong scattering occurs at the hypotenuse of a triangle shaped surface. In order to reduce the scattering from the edge, an anisotropic AIS can be used to control the direction of surface wave propagation, either toward or away from that edge. The rectangle patches, as the unit cell shown in Fig. 2, are patterned over the entire triangle region with various orientations. The rectangular patches are

rotated as a function of position on the surface to guide the surface waves to follow a controlled path along the surface. If rectangles are rotated gradually, the TM waves turn toward low impedance direction. If the rectangles are rotated abruptly, the surface waves may be reflected from the discontinuous boundaries between regions [16].

B. Dispersion

Since the TM surface wave mode is of interest, we analyzed the surface impedance by analyzing the refractive index for the TM mode [18]. The surface wave is bound to the surface when its propagation constant is larger than that in free space, or when the dispersion curve lies below the light line, as indicated in Fig. 2. The effective refractive index seen by the surface waves can be calculated [18]

$$n = k_t c/\omega \tag{1}$$

where k_t is the wavenumber of the surface wave, c is the speed of light, and ω is the angular frequency.

The dispersion characteristics shown in Fig. 2 are calculated using the eigenmode solver in Ansys HFSS. Periodic boundaries are applied to the four vertical walls of the simulation volume. Top and bottom faces are set with perfect electric boundaries. The height of the upper boundary to the unit cell is 25 mm. The red line represents the dispersion curve along the long edge of the dipole, i.e., x-direction, whereas the blue line shows the dispersion curve in short edge direction which is y-direction. It can be seen from Fig. 2 that impedance along x-axis gives high impedance (red curve), and in contrast, low impedance is achieved in y-axis (blue curve). The "light line" plotted in black corresponds to the speed of light in free space. The operating frequency is chosen at 15 GHz where the two primary directions have a large index contrast. For this structure, the effective refractive index varies from 1.2 in the y-direction to 2.0 in the x-direction.

For isotropic materials, k, B, and D are perpendicular, but for anisotropic materials, D and E are not always in parallel with each other. In dispersive materials, the group velocity and phase velocity of surface waves are different. Also, the direction of power flow or Poynting vector S and the direction of phase progression k may be different [31]. In the measured results, the propagation direction is determined by the wavefront, and the power flow is determined by the E field.

III. Pattern Design

Two patterning approaches are discussed in this section. One way is to pattern the rectangular unit cells onto the surface using discontinuous homogeneous regions. Alternatively, the other way is to pattern unit cells continuously, creating an inhomogeneous and smoothly varying impedance. Both of these methods are explored because anisotropic impedance surfaces are often difficult to pattern into arbitrary impedance functions while retaining high anisotropy due to the fact that the symmetry of the metal patches is lower than that of a simple square or triangular lattice. In other words, elongated metal shapes cannot be easily formed into smoothly curved paths. Thus, discrete regions of different impedances are much simpler to design in many cases, but may yield lower performance due to reflections from their interfaces. Here a simple square lattice with a dipole unit cell is chosen because it can be easily patterned into discontinuous or continuous patterns, and the results can be extrapolated to more complex unit cells.

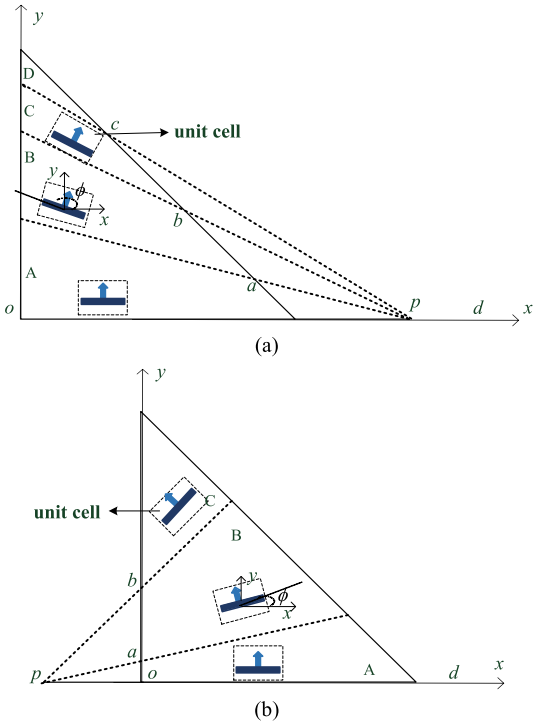

Fig. 3. Discontinuous design. The whole surface is divided into several sections. The rectangles are the homogeneous in each sector. (a) Anisotropic AIS guides the surface wave toward the hypotenuse edge. (b) Anisotropic AIS guides surface wave away from the edge.

A. Discontinuous Pattern

The simplest way to steer the surface waves toward or away from the edge is to refract them at a series of interfaces between discrete but homogeneous anisotropic regions. In these discontinuous cases, as shown in Fig. 3, the triangle is divided into several sections. Identical unit cells are used to fill up each section. Therefore, the entire triangular shape is patterned "discretely," which is the reason why we call it discontinuous patterns. For simplicity, a common point outside of the triangle is arbitrarily chosen, based on which three lines with the elevation angle from the horizontal direction as $\phi = 170°$, $160°$, and $150°$, respectively, are made to intersect with the triangular shape, dividing it into four sections. The common point p is shown in Fig. 3(a). $\angle apd$ is $170°$, $\angle bpd$ is $160°$, and $\angle cpd$ is $150°$. In Fig. 3, boundaries between sections are drawn in dotted line, and hypotenuse edges of triangles are drawn in solid line. Three unit cells are given as typical examples in Fig. 3, and the boundaries of the unit cells are drawn in dotted line. The bottom edge of each unit cell is in parallel with the section boundaries. If two different unit cells are overlapped on boundaries, in Fig.3, unit cells in

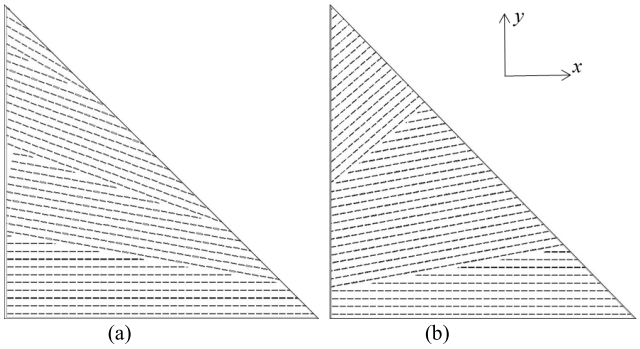

Fig. 4. Configuration of discontinuous designs. (a) Anisotropic AIS guiding surface waves toward the hypotenuse edge. (b) Anisotropic AIS guiding surface waves away from the edge.

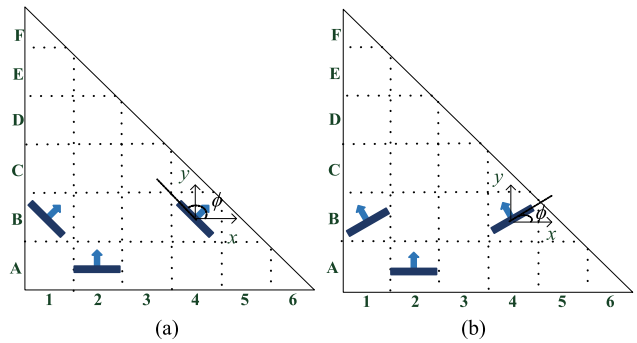

Fig. 5. Continuous design. The whole surface is divided into a square grid. The rotation angle of each cell varies according to the cell location. (a) Anisotropic AIS guiding surface waves toward the hypotenuse edge. (b) Anisotropic AIS guiding surface waves away from the edge.

region A are overrode by unit cells in region B, unit cells in region B are overrode by unit cells in region C, and so on. The rectangular metal patches in each section are identical in size and shape, but are oriented at different angles of 180°, 170°, 160°, and 150° in regions A, B, C, and D, respectively (the original position: the short edge of rectangle is in y-direction and the long edge is in x-direction in Fig. 2). Therefore, the longer edges of rectangular metal patches in each section are in parallel with section boundaries. As can be seen, the longer edges of the rectangular metal patches in region B are in parallel with the boundaries between region A, and region B. Thus, the low impedance direction approximates a continuous curve toward the hypotenuse of the triangle. The light blue arrows indicate direction of low surface refractive index.

In Fig. 3(b), the design is similar but the waves are intended to curve away from the edge. With the similar manner described above, the triangle is divided into three sections and the boundaries between them are at $\phi = 10°$ and 40°. $\angle apd$ is 10°, and $\angle bpd$ is 40°. The rectangles in each section are oriented to 0°, 10°, and 40° in regions A, B, and C, respectively, for this surface (the original position: the short edge of rectangle is in y-direction and the long edge is in x-direction in Fig. 2). The configuration of discontinuous designs are shown in Fig. 4.

Both of these are intended to be discontinuous approximations to the smoothly varying continuous surfaces to be described below. In both cases, the angles of the patches and the locations of the boundaries were chosen to minimize the scattering from the hypotenuse edge of the triangle. These discontinuous patterns produce extra reflections at their boundaries, as will be shown in Section IV. To reduce the reflections, continuous patterns are discussed in next section.

B. Continuous Pattern

As an alternative to the discontinuous case, a surface with the angle of low refractive index varies smoothly and continuously is also investigated. The unit cell studied here, in which a small rectangular dipole is arranged on a square lattice, is amenable to either type of patterning approach. However, more complex unit cells may be difficult to pattern in a continuous manner. Thus, it is important to understand and quantify the advantages relative to the discontinuous case.

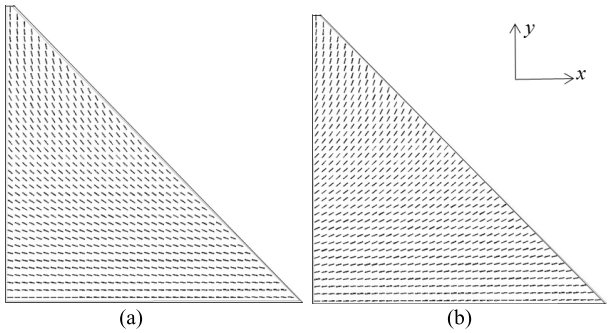

Fig. 6. Configuration of continuous design. (a) Anisotropic AIS guiding surface waves toward the hypotenuse edge. (b) Anisotropic AIS guiding surface waves away from the edge.

In order to reduce the reflections at the boundaries, continuous patterns are described in this section. In Fig. 5(a) and (b), the right angle vertices of the triangles are located on origin of our coordinate system. Instead of grouping the unit cells by several sections, all the unit cells are patterned in a much finer manner: dipole angle rotates by the row index. For example, as illustrated in Fig. 5(a) and (b), the triangle is filled up with six rows of unit cells, with row index A to F, and six columns with column index from one to six. Within each square, there is a single dipole unit cell. The direction of the diploe, described as the blue arrow in Fig. 5, rotates row by row, while maintains the same within each row. In Fig. 5(a), the metal patches are gradually rotated toward the hypotenuse edge, while in Fig. 5(b) they are gradually rotated away from it. For the case where the surface waves are directed to the hypotenuse [Fig. 5(b)], starting from the bottom row A, where the blue arrow is about perpendicular to the bottom edge, the direction of the blue arrow rotates gradually, and eventually get horizontal to the bottom edge as the last row (F as illustrated in Fig. 5). In contrast, the diploe direction also gets perpendicular to the bottom edge. For the case, the surface wave is directed away from the hypotenuse. The rotation step for each row is uniform. Therefore, in the following experimental demonstration, a surface with 40 rows of unit cells is designed, and the rotation step is 2.25°. The configuration of continuous designs is shown in Fig. 6.

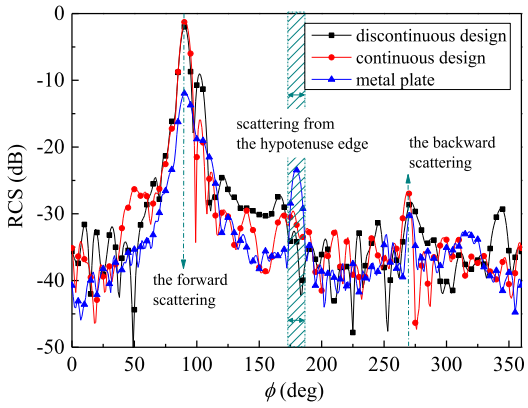

(a)

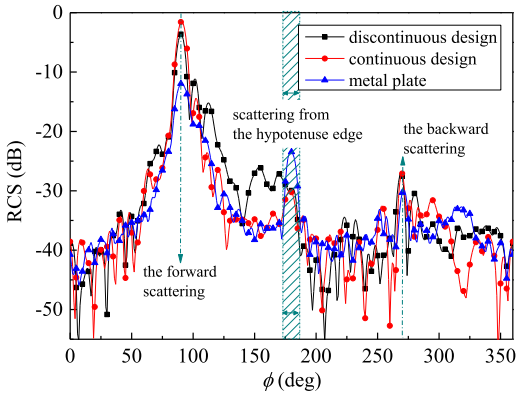

(b)

Fig. 7. Bistatic RCS of the bare metal triangle and the anisotropic impedance surfaces at 15 GHz. (a) Anisotropic AIS guiding surface waves toward the hypotenuse edge. (b) Anisotropic AIS guiding surface waves away from the edge.

With both patterns, the direction of surface wave propagation is curved and the scattering from the hypotenuse edge is reduced. Simulation results are discussed in the next section to compare the discontinuous pattern and the continuous pattern.

IV. Scattering Simulation

In this section, two aforementioned patterned triangle scatterers and a bare metal scatterer are examined by bistatic RCS simulation. Although the full bistatic RCS is simulated for the purpose of identifying other scattering characteristics, our primary concern is the scattering from the hypotenuse edge, and how much reduction is achieved by the proposed patterned surfaces. In this section, all of the triangular surfaces are 163 mm in width and 160 mm in length, and the unit cells are as described in Section II, and patterned as described in Section III. The surfaces are simulated using HFSS. Because the models are too complex to draw by hand, HFSS-MATLAB scripting is used to create the anisotropic impedance surface.

The scattering from a copper triangle is analyzed first. The bistatic RCS is shown in Fig. 7 and the relation between surface current and scattering is discussed. For the anisotropic AIS cases, the bistatic RCS is compared with the copper triangle, and the relation between current and scattering is discussed. Finally, the discontinuous case and continuous case are compared and discussed.

A. Bare Metal Surface

In this case, a simple copper triangle oriented in the xy plane is analyzed, and $\theta = 0°$ represents the z-direction, normal to the surface. In these simulations, a plane wave impinges on the copper triangle at an elevation angle of $\theta = 80°$ and azimuth angle of $\phi = 270°$. θ and ϕ are the parameters in the spherical coordinates. The bistatic RCS at $\theta = 80°$ elevation is the blue line shown in Fig. 7(a) and (b). We chose to analyze the RCS of all of the surfaces at a slight elevation angle (i.e., 10° from grazing) because the scattering from a thin metal sheet is negligible for TM polarization at grazing incidence. Note the three peaks in the scattering plot at $\phi = 90°$, $\phi = 180°$, and $\phi = 270°$. These correspond to forward scattering, reflection from the hypotenuse edge, and backward scattering, respectively. We are not concerned with the large forward scattering peak at $\phi = 90°$, nor the smaller backward scattering peak at $\phi = 270°$, but only with the peak at $\phi = 180°$ representing the edge which we are attempting to control. As we will discuss below, both patterning methods are able to provide reduction of the specular reflection from the hypotenuse edge, with varying degrees of additional scattering to other directions.

B. Patterned Metal Surfaces

Fig. 7(a) compares the metal triangle with two patterned triangles using the discontinuous and continuous patterning methods, both of which intend to bend the surface currents toward the hypotenuse edge. For both cases, the patterned surfaces show reduced scattering compared to the metal surface, with a reduction of about 8 dB for the continuous pattern and 10 dB for the discontinuous case. Fig. 7(b) shows the same results but for the cases where the patterned surfaces are intended to bend the surface currents away from the hypotenuse edge. In these cases, both approaches reduce the bistatic RCS at $\phi = 180°$ by about 7 dB, demonstrating both approaches (steering the wave toward or away from the edge) change the phase progression along that edge, and thus reduce the specular reflection at $\phi = 180°$. However, two points are noted: 1) All four cases still show lobes at or near $\phi = 180°$, and the location and level of these lobes can significantly affect the actual degree of improvement. Thus, one should be careful to draw conclusions based on one curve being 1–2 dB above another, and instead we should discuss the overall trend. Because the scattering to any angle is a result of the integrated reflection from the entire surface, small variations can determine whether different components add or cancel at a particular angle. Thus, these RCS plots must be compared with other simulation approaches and measurement results to verify and quantify this approach and 2) Overall, both types of patterning approaches show the same trends, but the discontinuous surfaces have a higher degree of diffuse scattering, particularly at angles below $\phi = 45°$ in Fig. 7(a), and between $\phi = 90°$ and 180° in both figures. The scattering in Fig. 7(a) below $\phi = 45°$ is due to the orientation of the

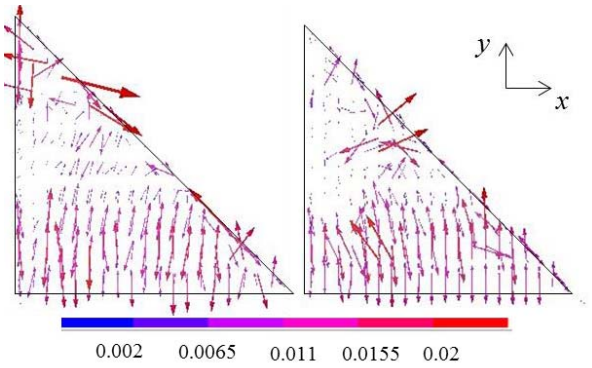

Fig. 8. Surface currents on the discontinuous anisotropic impedance surfaces designed to guide the surface currents at 15 GHz (a) toward the edge or (b) away from the edge. Note the regions of high field at the boundaries between regions.

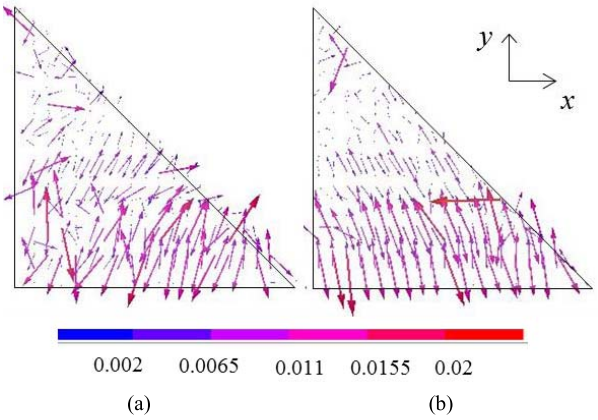

Fig. 9. Surface currents on the continuous anisotropic impedance surfaces designed to guide the surface currents at 15 GHz (a) toward the edge or (b) away from the edge. Note that the fields are much more uniform than in the discontinuous case.

edges in the discontinuous structure. The continuous structure also shows a lobe near $\phi = 45°$ which may be because we have bent the surface waves in precisely that direction. However, as with the prior point above, assigning particular lobes to specific regions of the surface can be difficult due to the complex nature of scattering from an electrically large object. The main point to take away from this data is that using anisotropic impedance surfaces to change the angle at which surface waves impinge on an edge can affect the scattering from that edge, and that there appears to be a slight advantage to using slowly varying impedance functions in terms of not generating other artifacts from discontinuities.

The differences between the discontinuous and continuous designs can also be seen in the simulated field plots in Figs. 8 and 9. The incident plane wave is the same as in Fig. 7. The discontinuous designs in Fig. 8 show regions of high fields at the boundaries between regions, which are likely to cause scattering, and which are not seen in the continuous designs in Fig. 9.

V. Measurements

The anisotropic impedance surfaces are fabricated as shown in Fig. 10. The unit cells are printed on 1.27 mm thick Rogers

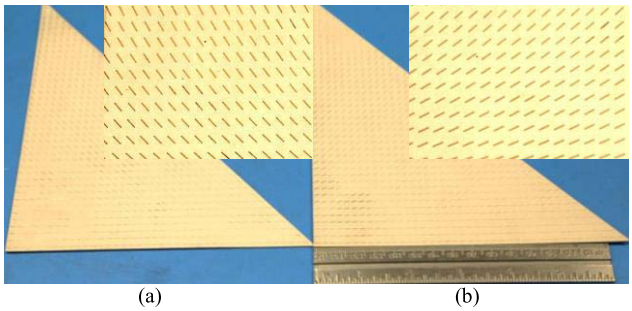

Fig. 10. Anisotropic impedance surface fabrication. The samples are 163 mm in width and 160 mm in length. (a) Surface for steering toward the edge. (b) Surface for steering away from the edge.

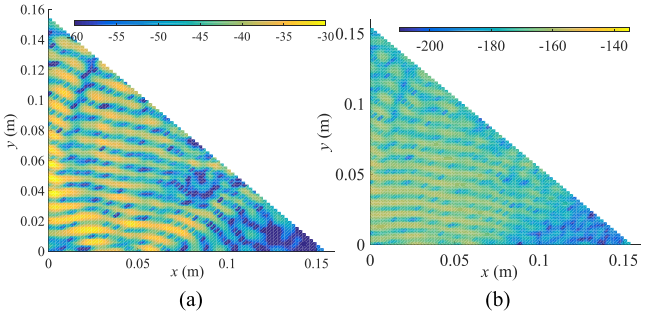

Fig. 11. Near-field plot of the surface waves on the patterned surface designed to steer the waves toward the hypotenuse at 15 GHz. (a) Raw measured data. (b) Transformed data.

6010 which has a relative dielectric constant of 10.2, with a metal ground plane on the back side.

A. Near-Field Measurement

If a surface charge density wave radiates into the far field, the magnitude of wave vector parallel to the propagation direction should be lower than the magnitude of the wave vector in free space [31]. If not, the wave decays in the direction perpendicular to the surface, and is described as a bound wave.

A surface wave was launched on each surface using an H-plane sectoral horn antenna placed near the edge of the surface. Near-field data are collected using a probe connected to an Agilent E5071C vector network analyzer, and the probe is scanned over the surface at a height of 2–3 mm, with data taken every 2 mm over the surface. Figs. 11(a) and 12(a) show the raw measurement results for the E-field in the z-direction.

The probe measures the E_z field including both surface wave and incident wave over the anisotropic surface. In order to distinguish the surface wave from the incident wave, measurement data are transformed to the k domain. The coefficient of imaginary propagation constant in the z-direction in the k domain can be used and transformed to the spatial domain by taking its Fourier transform. If the E-field on the xy plane ($z = d$) is known, the E-field above the $z = d$ plane can be calculated by the following equations [27]:

$$E_z = \iint A_z(k_x, k_y) e^{-j(k_x x + k_y y)} dk_x dk_y \quad (2)$$

$$A_z(k_x, k_y) = \frac{1}{4\pi^2} \iint E_z(x, y) e^{j(k_x x + k_y y)} dx dy. \quad (3)$$

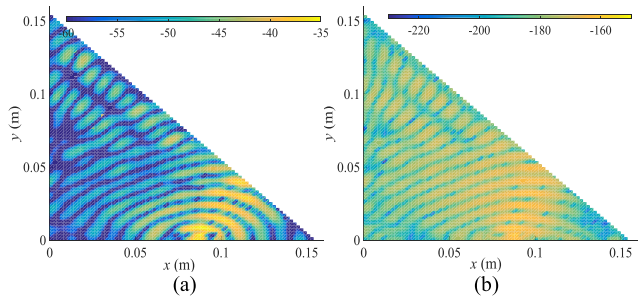

Fig. 12. Near-field plot of the surface waves on the patterned surface designed to steer the waves away from the hypotenuse at 15 GHz. (a) Raw measured data. (b) Transformed data.

Fig. 13. Far-field measurement setup for bistatic RCS measurements. The source horn antenna is fixed on a tripod and the receive horn antenna is rotated around the surface under test.

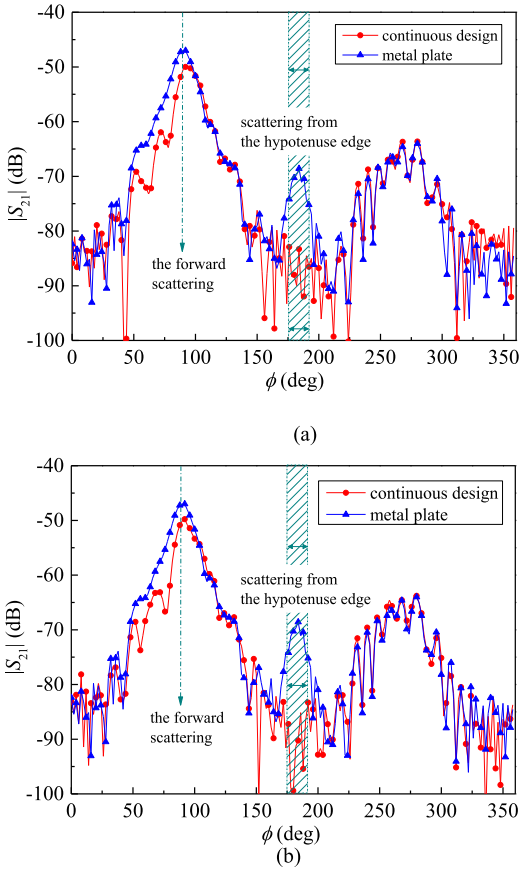

Fig. 14. S_{21} measurement at 15 GHz results for (a) surface designed to steer toward the hypotenuse edge and (b) surface designed to steer away from the hypotenuse edge.

This has the effect of filtering out the data that do not correspond to a bound surface wave, and removes the interference caused by free space waves which are also excited by the feed horn, resulting in cleaner plot of only the surface wave. The method is similar to the near-field to far-field transformation [28]–[30]. In the results shown in Figs. 11(b) and 12(b), curved surface waves can be clearly observed.

B. Bi-Static RCS Measurements

The bistatic RCS measurements were performed in an anechoic chamber with the setup shown in Fig. 13 using an Agilent E5071C vector network analyzer (VNA), a rotating platform, and a pair of horn antennas, one of which was an H-plane sectoral horn. Although this test was not ideal, and large facilities exist for performing bistatic RCS measurements, those are not available to us at reasonable cost. Thus, these experiments represent a quick and simple method to obtain an approximate bistatic RCS in a relatively small chamber. Remarkably, they provide results that are qualitatively and quantitatively in line with the simulations in Fig. 7. To perform this measurement, the surface to be tested was hanging in the chamber at a fixed location by a thin dielectric wire. The source horn was stationary, about 1.5 m from the surface, and this generates the incident plane wave. It was placed on an adjustable tripod so that the angle of the incident wave can be controlled. The receive antenna was mounted on an arm which was attached to a rotating pedestal, and rotated around the stationary surface under test. The measurement is limited by the directionality of the receive antenna because it is within the main beam of the source antenna, so the side-lobes from itself can contribute to the measured RCS of the surface at certain angles. It is also limited by the distance of the receive antenna from the surface which is not strictly within the far field. (Note that the distance between the source horn and target is 1.5 m, the distance between the receive horn and target is 0.5 m, and the distance of far field is 2.56 m). Nonetheless, this is a direct, if limited, measurement of the bistatic RCS, and thus provides useful data that are not available from simulations or other indirect measurement methods.

The plots in Fig. 14 show the S_{21} data from the measurement with the receiver antenna rotating over a complete circle. The blue line indicates the scattering from the copper triangle surface and the red line indicates the scattering from the anisotropic impedance surface. Compared to the copper triangle surface, the scattering from both patterned surfaces is reduced significantly in the direction corresponding to reflection from the hypotenuse edge, at 180°. Moreover, the relative improvement is on the order of what has been seen in the simulations, roughly 10 dB.

We must be careful not to draw inappropriate conclusions from Fig. 14, because it is not a true bistatic RCS measurement, and is confounded by the limitations discussed above. For this reason, it cannot be compared directly to Fig. 7. For example, the magnitude of the peak at $\phi = 90^\circ$ is a function of the gain of the two horns and their separation, not a direct indication of the magnitude of the RCS, which would require a calibrated target. Furthermore, the large set of lobes at $\phi = 270^\circ$ may be due as much to the back lobe of the receive horn as any properties of the surface. Reflections from the back wall of the chamber would also be maximized at this angle. The $\phi = 180^\circ$ case is the angle where the receive horn is oriented orthogonally to the transmit horn, so it is expected to have a low gain in that direction, and reflections from the chamber walls would be at a minimum. Thus, in spite of the limitations of this measurement, the distinct elimination of the scattering peak at $\phi = 180^\circ$ in both patterned surfaces, corresponding to the angle of specular reflection from the hypotenuse edge, may be taken as additional confirmation that this method provides a useful way to manipulate reflection from edges.

VI. Conclusion

An anisotropic impedance surface method is proposed for reducing specular reflection from edges by steering surface waves to change the direction at which they impinge on the edge. As an example, a triangular surface designed with a clearly identifiable scattering peak from the hypotenuse edge, and inhomogeneous anisotropic impedance surfaces are designed to reduce scattering from that edge. A simple unit cell containing a rectangular metallic dipole element is chosen which provides high anisotropy and can be rotated to any direction without interfering with neighboring cells. A triangular sample is patterned with anisotropic impedance surfaces based on both discontinuous and continuous designs. Simulation data suggest that both approaches provide similar reduction in specular reflection from the edge, but the discontinuous design suffers from higher scattering at other angles compared to the continuous design. This is verified by field plots on the surface which show hot spots at the discontinuities between regions. Fabricated samples clearly demonstrate steering of the surface waves in near-field scans. For both types of surfaces, steering the waves either toward or away from the hypotenuse edge shows a clear reduction of the scattering peak from that edge in simple bistatic RCS measurements. This represents a new approach that can be incorporated into designs of antennas, reflectors, or other structures to manipulate specular reflections for applications such as reducing coupling between antennas, eliminating unwanted lobes, or otherwise manipulating the radiation properties of structures. It is worth noting that energy that is diverted from specular scattering can end up as diffuse scattering, spread over other angles. Thus, designs which incorporate this technique must be careful to control for the range of angles at which the waves impinge on any edges, and the effect on the overall scattering profile. Furthermore, this paper only provides a narrowband solution based on a passive AIS, but there is current research aimed at building broadband impedance surfaces using active circuit approaches [33].

Acknowledgment

The authors would like to thank their colleague R. Quarfoth for the contribution to the measurement.

References

[1] J. Zhang, J. Wang, M. Chen, and Z. Zhang, "RCS reduction of patch array antenna by electromagnetic band-gap structure," *IEEE Antennas Wireless Propag. Lett.*, vol. 11, pp. 1048–1051, 2012.

[2] W. Xu, J. Wang, M. Chen, Z. Zhang, and Z. Li, "A novel microstrip antenna with composite patch structure for reduction of in-band RCS," *IEEE Antennas Wireless Propag. Lett.*, vol. 14, pp. 139–142, 2015.

[3] W. Chen, C. A. Balanis, and C. R. Birtcher, "Checkerboard EBG surfaces for wideband radar cross section reduction," *IEEE Trans. Antennas Propag.*, vol. 63, no. 6, pp. 2636–2645, Jun. 2015.

[4] H. Ming, Y. Shuwen, G. Fei, R. Quarfoth, and D. Sievenpiper, "A 2-D multibeam half Maxwell fish-eye lens antenna using high impedance surfaces," *IEEE Antennas Wireless Propag. Lett.*, vol. 13, pp. 365–368, 2014.

[5] M. Bosiljevac, M. Casaletti, F. Caminita, Z. Sipus, and S. Maci, "Non-uniform metasurface luneburg lens antenna design," *IEEE Trans. Antennas Propag.*, vol. 60, no. 9, pp. 4065–4073, Sep. 2012.

[6] R. Yang, Z. Lei, L. Chen, Z. Wang, and Y. Hao, "Surface wave transformation lens antennas," *IEEE Trans. Antenna Propag.*, vol. 62, no. 2, pp. 973–977, Feb. 2014.

[7] B. Fuchs, O. Lafond, S. Rondineau, and M. Himdi, "Design and characterization of half Maxwell fish-eye lens antennas in millimeter waves," *IEEE Trans. Microw. Theory Techn.*, vol. 54, no. 6, pp. 2292–2300, Jun. 2006.

[8] R. Quarfoth and D. Sievenpiper, "Artificial tensor impedance surface waveguides," *IEEE Trans. Antennas Propag.*, vol. 61, no. 7, pp. 3597–3606, Jul. 2013.

[9] Y.-Q. Li, H. Zhangm, Y.-Q. Fu, and N.-C. Yuan, "RCS reduction of ridged waveguide slot antenna array using EBG radar absorbing material," *IEEE Trans. Antennas Propag. Lett.*, vol. 7, pp. 473–476, 2008.

[10] H.-K. Jang, J.-H. Shin, and C.-G. Kim, "Low RCS patch array antenna with electromagnetic bandgap using a conducting polymer," in *Proc. Int. Conf. Electromagn. Adv. Appl. (ICEAA)*, Sep. 2010, pp. 140–143.

[11] J. C. I. Galarregui, A. T. Pereda, J. L. M. de Falcón, I. Ederra, R. Gonzalo, and P. de Maagt, "Broadband radar cross-section reduction using AMC technology," *IEEE Trans. Antennas Propag.*, vol. 61, no. 12, pp. 6136–6143, Dec. 2013.

[12] M. Paquay, J. C. Iriarte, I. Ederra, R. Gonzalo, and P. D. Maagt, "Thin AMC structure for radar cross-section reduction," *IEEE Trans. Antennas Propag.*, vol. 55, no. 12, pp. 3630–3638, Dec. 2007.

[13] A. M. Patel and A. Grbic, "Transformation electromagnetics devices based on printed-circuit tensor impedance surfaces," *IEEE Trans. Microw. Theory Techn.*, vol. 62, no. 5, pp. 1102–1111, May 2014.

[14] R. Quarfoth and D. Sievenpiper, "Surface wave scattering reduction using beam shifters," *IEEE Antennas Wireless Propag. Lett.*, vol. 13, pp. 963–966, 2014.

[15] F. C. Smith, "Edge coatings that reduce monostatic RCS," *IEE Proc. Radar, Sonar Navigat.*, vol. 149, no. 6, pp. 310–314, Dec. 2002.

[16] R. Quarfoth and D. Sievenpiper, "Alteration of electromagnetic scattering using hard and soft anisotropic impedance surfaces," *IEEE Trans. Antennas Propag.*, vol. 63, no. 10, pp. 4593–4599, Oct. 2015.

[17] H. J. Bilow, "Guided waves on a planar tensor impedance surface," *IEEE Trans. Antennas Propag.*, vol. 51, no. 10, pp. 2788–2792, Oct. 2003.

[18] B. H. Fong, J. S. Colburn, J. J. Ottusch, J. L. Visher, and D. Sievenpiper, "Scalar and tensor holographic artificial impedance surfaces," *IEEE Trans. Antennas Propag.*, vol. 58, no. 10, pp. 3212–3221, Oct. 2010.

[19] A. M. Patel and A. Grbic, "Modeling and analysis of printed-circuit tensor impedance surfaces," *IEEE Trans. Antennas Propag.*, vol. 61, no. 1, pp. 211–220, Jan. 2013.

[20] J. H. Wang and Y. B. Gan, "In-band scattering of dipole array with edge loaded rectangular reflector," in *Proc. IEEE Antennas Propag. Soc. Int. Symp.*, Jun. 2003, pp. 468–471.

[21] J. M. Usoff and B. A. Munk, "Edge effects of truncated periodic surfaces of thin wire elements," *IEEE Trans. Antennas Propag.*, vol. 42, no. 7, pp. 946–953, Jul. 1994.

[22] D. J. Gregoire and A. V. Kabakian, "Surface-wave waveguides," *IEEE Antennas Wireless Propag. Lett.*, vol. 10, pp. 1512–1515, 2011.

[23] E. Doumanis, G. Goussetis, J. L. Gómez-Tornero, R. Cahill, and V. Fusco, "Anisotropic impedance surfaces for linear to circular polarization conversion," *IEEE Trans. Antennas Propag.*, vol. 60, no. 1, pp. 212–219, Jan. 2012.

[24] S. Maci and P. Kildal, "Hard and soft gangbuster surface," in *Proc. Int. Symp. Electromagn. Theory (URSI EMTS)*, pp. 290–292, 2004.
[25] S. Maci, M. Caiazzo, A. Cucini, and M. Casaletti, "A pole-zero matching method for EBG surfaces composed of a dipole FSS printed on a grounded dielectric slab," *IEEE Trans. Antennas Propag.*, vol. 53, no. 1, pp. 70–81, Jan. 2005.
[26] J. A. Aas, "Plane-wave reflection properties of two artificially hard surfaces," *IEEE Trans. Antennas Propag.*, vol. 39, no. 5, pp. 651–656, May 1991.
[27] R. Yang, S. Zhang, J. Jin, C. Lu, and W. Yu, *Advanced Electromagnetic Theory*. Beijing, China: Higher Education Press, 2008, pp. 218–219.
[28] R. A. Marr, U. H. W. Lammers, T. B. Hansen, T. J. Tanigawa, and R. V. McGahan, "Bistatic RCS calculations from cylindrical near-field measurements—Part II: Experiments," *IEEE Trans. Antennas Propag.*, vol. 54, no. 12, pp. 3857–3864, Dec. 2006.
[29] T. B. Hansen, R. A. Marr, U. H. W. Lammers, T. J. Tanigawa, and R. V. McGahan, "Bistatic RCS calculations from cylindrical near-field measurements—Part I: Theory," *IEEE Trans. Antennas Propag.*, vol. 54, no. 12, pp. 3846–3856, Dec. 2006.
[30] O. M. Bucci and C. Gennarelli, "Use of sampling expansions in near-field-far-field transformation: The cylindrical case," *IEEE Trans. Antennas Propag.*, vol. 36, no. 6, pp. 830–835, Jun. 1998.
[31] A. M. Patel and A. Grbic, "The effects of spatial dispersion on power flow along a printed-circuit tensor impedance surface," *IEEE Trans. Antennas Propag.*, vol. 62, no. 3, pp. 1464–1469, Mar. 2014.
[32] S. Sun, Q. He, S. Xiao, Q. Xu, X. Li, and L. Zhou, "Gradient-index meta-surfaces as a bridge linking propagating waves and surface waves," *Nature Mater.*, vol. 11, no. 5, pp. 426–431, 2012.
[33] J. Long and D. Sievenpiper, "Low-profile and low-dispersion artificial impedance surface in the UHF band based on non-foster circuit loading," *IEEE Trans. Antennas Propag.*, vol. 64, no. 7, pp. 3003–3010, Jul. 2016.

Haijian Hou received the B.S. degree in communication engineering from Beijing Jiaotong University, Beijing, China, in 2012, where she is currently pursuing the Ph.D. degree in engineering.

Her current research interests include scattering in time domain from metamaterials, FSS, and antennas.

Jiang Long (S'11) received the B.S. and M.S. degrees from Zhejiang University, Hangzhou, China, in 2007 and 2010, respectively, and the Ph.D. degree from the University of California, San Diego, CA, USA, in 2015.

He is currently an RF Engineer with Skyworks Solution Inc., Woburn, MA, USA. His current research interests include nonfoster circuits in antenna/microwave applications, including nonfoster circuit loaded active fast-wave waveguides, broadband metasurfaces, broadband antennas, and active microwave components.

Dr. Jiang was awarded the IEEE MTT-S Graduate Fellowship in 2015.

Junhong Wang (M'02–SM'03) was born in Jiangsu, China, in 1965. He received the B.S. and M.S. degrees in electrical engineering from the University of Electronic Science and Technology of China, Chengdu, China, in 1988 and 1991, respectively, and the Ph.D. degree in electrical engineering from Southwest Jiaotong University, Chengdu, in 1994.

In 1995, he joined the Department of Electrical Engineering, Beijing Jiaotong University, Beijing, China, as a Faculty Member, where he became a Professor in 1999. From 1999 to 2000, he was a Research Associate with the Department of Electric Engineering, City University of Hong Kong, Hong Kong. From 2002 to 2003, he was a Research Scientist with the Temasek Laboratories, National University of Singapore, Singapore. He is currently with the Key Laboratory of all Optical Network and Advanced Telecommunication Network, Ministry of Education of China, Beijing Jiaotong Univeristy, and also with the Institute of Lightwave Technology, Beijing Jiaotong University. His current research interests include numerical methods, antennas, scattering, and leaky wave structures.

Daniel F. Sievenpiper (M'94–SM'04–F'09) received the B.S. and Ph.D. degrees in electrical engineering from the University of California, Los Angeles, CA, USA, in 1994 and 1999, respectively.

He was the Director of the Applied Electromagnetics Laboratory, HRL Laboratories, Malibu, CA, USA, where he was involved in artificial impedance surfaces, conformal antennas, tunable and wearable antennas, and beam steering methods. He is currently a Professor with the University of California, San Diego, CA, USA, where he is involved in antennas and electromagnetic structures. He has authored or co-authored more than 100 technical publications and holds more than 70 issued patents.

Dr. Sievenpiper was awarded the URSI Issac Koga Gold Medal in 2008. He has been an Associate Editor of the IEEE *Antennas and Wireless Propagation Letters* since 2010.